scientific reports

Check for updates

OPEN

Optimization of heat transfer in a double lid-driven cavity with isoperimetric heated blocks using GFEM

Ahmed Refaie Ali[1,4]✉, Rashid Mahmood[2], Maria Ishfaq[2], Nusrat Rehman[2] & Afraz Hussain Majeed[3]

This article is concerned with the examination of flow dynamics and heat transfer characteristics in a 1:4 double lid driven cavity in presence of isoperimetric heated blocks of various shapes. The focus is to identify the optimal shape that enhances the heat transfer in a tall cavity. The parametric settings are chosen in such a way that all the convection regimes including natural, forced and mixed convection could be generated. This cavity has lids positioned at the top and bottom, moving in opposite directions along the x-axis. The physical system is represented as a set of coupled partial differential equations incorporating the rheological properties of the power-law fluids (PL). The governing equations in conjunction with various non-dimensional physical parameters are simulated via Galerkin's Finite Element Method (GFEM) on a very fine hybrid grid. The study includes the computation of the Kinetic Energy and Average Nusselt number to determine the optimal shape. It is concluded that the circular block is superior to the other two in terms of heat transmission efficiency.

Keywords Mixed convection, Lid driven cavity, Non-Newtonian fluid, Isoperimetric, FEM computation, Kinetic energy

List of symbols

AR	Aspect ratio
C_p	Specific heat
g	Gravitational acceleration
Gr	Grashof number, dimensionless.
H	Height of the cavity
K	Thermal conductivity
L	Length of the cavity
n	Power-law index, dimensionless
N_u	Local Nusselt number, dimensionless
p	Pressure
$\overline{P}$	Dimensionless pressure
Pr	Prandtl number, dimensionless
Re	Reynolds number, dimensionless
Ri	Richardson number, dimensionless
T	Temperature
U_{lid}	Velocity of the moving walls
u, v	Velocity in X and Y direction
$U, \overline{V}$	Dimensionless velocity in X and Y direction

Greek symbols

β	Thermal expansion coefficient
ρ	Fluid density

[1]Department of Mathematics and Computer Science, Faculty of Science, Menoufia University, Shebin El Kom 32511, Menofia, Egypt. [2]Department of Mathematics, Air University, PAF Complex E-9, Islamabad 44000, Pakistan. [3]School of Energy and Power Engineering, Jiangsu University, Zhenjiang 212013, China. [4]Department of Mathematics, Faculty of Science, New Mansoura University, New Mansoura City 35742, Egypt. ✉email: ahmed.refaie@science.menofia.edu.eg

η Apparent viscosity
θ Normalized temperature, dimensionless
μ Dynamic viscosity
υ Kinematic viscosity

Subscripts

C Cold
H Hot

Convection in cavities is a well-studied area in fluid mechanics, and there is a vast literature on this topic. Temperature variations and movements of the walls of enclosure give rise to buoyancy-driven and forced convection flow, which in turn generated mixed convection flow features. The motion of the fluid can be driven by natural convection, forced convection, or a combination of both[1,2]. The research of free convection within the cavity is among the most fundamental principles around the areas of science. The flow of the fluid and the transmission of heat qualities in different types of cavities, including square, rectangular, and circular forms, have been utilized by researchers to observe natural and forced convection. In addition to that, forced convection, which is produced on by an outside flow or a moving boundary wall, scientists have also researched on natural convection within the domain. This study has plenty of multiple applications that can be found in our daily life. For example, the phenomenon used in room ventilation and the apparatus used in cooling machines and many more.

G. DE Davis[1] has examined laminar natural convection in a long rectangular domain, he also estimated behavior of free convection in a square air cavity having sidewall that are not heated equally[2]. S.Roy[3] conducted an investigation on a square cavity to see the behavior in the motion of free convection due to the effect of uniformly and non-uniformly heated wall(s). Mixed convection research was done Selimefendigil and Öztop[4] in a L-shaped wall moving domain of a nano-fluid which was done by changing the inclination angle, solid volume percentage, and Hartmann number to generate the internal heat. In a long, air-filled hollow domain with an aspect ratio of 16, Zhu and Yang[5] quantitatively examined the emigrating natural convection for various Rayleigh numbers.In a long and double wall-driven domain the mixed convection with differential heating is researched by Öztop and Dagtekin[6]. It was discovered that the rate of heat transfer increased when the walls moved in the opposite direction. In upright chambers that have noticeably hot walls and contain air as a fluid that have variety of aspect ratios, Wakitani[7] predicted the natural convection flow pattern. It was discovered that the essential Rayleigh number decreases due to the aspect ratio. In a tall, quadrilateral structure, Rayleigh-Bernard convection was investigated by D'Orizo et al.[8]. Latterly Lartigue[9] explained auxiliary flow production in a long cavity of aspect ratio equals to 40, where he noted that displacement areas shift to the cavity's descending zone at Ra = 9222. Subsequently, Basak et al.[10] investigated mixed convection flows inside a cavity with uniform and non-uniform heating of the lower walls of the cavity.

Moreover, Javed et al. conducted an experiment in a uniformly and unevenly warm lower walls of a four-sided polygon cavity to analyze magnetohydrodynamics mixed convection. It is discovered that the enclosure exhibits stronger circulation and a dominating convection effect as the Rayleigh number rises[11]. Similarly, Lamsaadi[12] looked at the natural convection in long quadrilateral domains for various non-Newtonian fluids and values of Prandtl from $1 \leq Pr \leq 100$, better heat transfer rates have been observed in shear-thinning fluids. Likewise, Mendu and Das[13] investigated forced convection for different governing parameters in a dual lid driven cavity with non-Newtonian fluids. The probability of secondary vortex production declines as the power-law index increases. In a slanted penetrable, open-ended, insignificant hollow cavity Raizah et al.[14] computationally conducted a buoyancy-driven convection for non-Newtonian fluids. He concluded that the increase in aspect ratio reduces the amount of heat transmission rate.

Souayeh et al.[15] conducted a numerical study on steady, laminar natural convection within a two-dimensional enclosure filled with water and containing a rectangular conducting body. Their findings demonstrate that a vertical orientation of the body results in superior heat transfer compared to a horizontal configuration. Souayeh et al.[16] investigate the impact of varying inclination angles of a low-temperature cubical enclosure on the flow structure and heat transfer rate, with a high-temperature inner circular cylinder. Their findings reveal that the heat transfer rate increases with higher Rayleigh numbers. Souayeh et al.[17] analyzed the impact of velocity ratio and the radius size of an inner semicircle placed at the bottom wall of a two-sided, non-facing lid-driven cavity on bifurcation phenomena. Their numerical results are integrated into a detailed correlation between the critical Reynolds number and various other parameters. Hammami et al.[18] conduct a numerical investigation of a two-sided lid-driven cubic cavity with a cylindrical shape placed at its center. Their study reveals that as the Reynolds number increases up to 1500, the moving parallel lids generate vortices in the rear planes of the cavity behind the cylinder. Souayeh et al.[19] conduct a systematic numerical investigation using the finite volume method combined with a full multigrid technique to study the two-dimensional and three-dimensional flow of an incompressible fluid within a cavity driven by the motion of the upper lid. Their findings conclude that a bidimensional cavity with an inner circle at the center exhibits a higher critical Reynolds number compared to one without the inner circle, leading to a delay in flow unsteadiness.

While referring to K.M. Gangawane's work[20], an investigation was conducted utilizing numerical techniques resulting from mixed convection in a quadrilateral domain to examine the dynamics of transfer of heat and flow of the fluid. In this study, motion was imparted to one of the vertical walls, while a centrally positioned elliptical block was heated to maintain a stable condition. The primary aim of this research was to investigate the impacts of various flow parameters, for instance the vertical wall's direction of motion (either up or down along the y-coordinate axis) and the elliptical cylinder's aspect ratio (0.5, 1, 2). Numerous dimensionless numbers were investigated, including $Gr\ (1-100)$, $Pr\ (1-100)$, and $Re\ (1-5000)$, respectively. The finite volume technique (FVM) and the SIMPLE numerical methodology were used in the simulations. To acquire a complete knowledge

of the enclosure's physical behavior, the inquiry included a rigorous assessment of streamline and isotherm profiles. Additionally, the study calculated the Nusselt number (Nu) for circular shape and elliptical cylinder and compared the average rate of heat transmission of both the cases. The findings exhibit that the rate of thermal transmission has a more substantial effect due to the motion of the walls as compared to the size of the elliptical cylinder. Furthermore, it was observed that the cavity which contains a vertically upward moving wall exhibited an enhanced heat transfer rate. The domain with a heated elliptical block ($Er \neq 1$) has high rate of thermal transmission convection in comparison with the one which has a purely circular shape.

Elboughdiri et al.[21] visualized thermal energy within an Oldroyd-B fluid model by incorporating different types of nanoparticles to enhance thermal performance. Their findings indicate that increasing Eckert number, magnetic number, solar thermal radiation number, and electric field number leads to improved temperature profiles. Sohail et al.[22] explored the application of a tetra-hybrid nanofluid (containing aluminum oxide, iron dioxide, titanium dioxide, and copper) in a crossflow model over a vertical disk. Their study considered the impact of nanoparticle shapes (bricks, cylindrical, and platelets), the influence of electro-magneto-hydrodynamic effects, and the effect of quadratic thermal radiation. Their findings suggest that tetra-hybrid nanofluids offer a significant advantage in industrial applications demanding the highest thermal energy production. Elboughdiri et al.[23] conducted a mathematical analysis of dual simulations involving tangent hyperbolic rheology, heat transfer, and mass diffusion on an expanding/shrinking needle. Incorporating Darcy's Forchheimer law and a magnetic field, their study revealed that increasing chemical and Schmidt numbers led to a decrease in concentration profiles. Sohail et al.,[24] implemented finite element method to simulate the hybrid nanofluid model in a Riga plate and compared the thermal performance of the system.

Numerical analysis is conducted in a wall moving domain by Billah, M. M., et al. [25] to investigate the phenomenon of thermal transmission due to mixed convection, where a hot empty cylinder is placed in the middle of the cavity. Billah, M. M., et al. Conducted this study to simulate realistic systems such as ovens that have heaters and air-conditioned electrical equipment. To solve the governing equations, a Newton–Raphson algorithm combined with a Galerkin's weighted residual finite scheme is utilized. The calculations encompass a broad spectrum of ratio of thermal conductive solids and fluids, diameters of cylinders and Richardson numbers The findings are shown through the pictorial representation of average Nusselt number, temperature contours, velocity profiles and streamlines on the heated surface, and different specified parameters are considered in the domain of thermally distributive fluid. It is noted that substantial sensitivity to the diameter of a cylinder as well as the ratio of heat conductivity of solid fluid have been displayed by the distribution of temperature and field of flow in the three convective regimes. Islam et al. have quantitatively examined the features of a square obstruction which is heated at equilibrium temperature to analyze the properties of mixed convection inside a four-sided closed domain. The cavity consists of obstructions that are located at its upper left and lower right edges to provide the best heat transmission results which is determined by the Nusselt number[26]. Numerical results for non-Newtonian fluids in a double, wall-moving quadrilateral domain with a decentered heated triangular obstacle having a constant temperature, have been presented by Manchanda and Gangawane[27]. For fluids with $n = 0.2$, it was discovered that the impact of the mixed convection variables had little bearing on the fluid and thermal structure inside the cavity. Vijayan and Gangawane[28] did computational study to investigate the movement of fluids and transfer of heat characteristics resulting from combination of forced and free convection in a long wall moving domain holding an equally heated equilateral triangular block. The division of fluid and its structural behavior in the cavity becomes increasingly erratic as the aspect ratio (AR) of the enclosure increases. Thus, when the aspect ratio of the considered space grows larger, the distribution of fluid and its structural behavior within the cavity becomes more scattered. In a study by Cheng et al.[29], the authors investigated the features of heat transfer through mixed convection in a wall moving square cavity, considering different Richardson and Prandtl numbers. The researchers present a temporal analysis of the kinetic energy and average Nusselt number, demonstrating the progression from laminar to chaotic flows. The experiments were conducted with a horizontal orientation, Laidoudi and Ameur[30] quantitatively investigated mixed convection between two revolving circular cylinders. The outcomes for various Prandtl-Richardson numbers, fluid index, and Reynold values have also been depicted. In a two-dimensional hollow having a sliding lid, mixed (combined) convective non-Newtonian fluid flow is numerically simulated by Thoura et al. in[31]. where he discovered that the standard deviation of thermal transmission rate decreases as the Richardson number is incremented for a particular skew angle. Using a fillet square cavity as a model, Rehman et al.[32] performed a numerical analysis of a magnetized ferric oxide–water nanofluid. It can be inferred that the fluid flows over the cylinder as it revolves in a clockwise direction. Furthermore, increasing ferroparticle volume and angular velocity increases Nusselt number and reduces thermal and viscous entropy. Similarly, Safaei.et al.[33] conducted a mathematical investigation on a square domain with cold right and left walls, an adiabatic upper wall in motion, and a heated bottom wall held fixed. It is discovered that the isothermal lines, which govern natural convection, are essentially symmetric, and that as forced convection progresses, these lines become asymmetric. In a discretely heated wall-driven domain, Roy et al.[34] explored different power-law fluids along with their thermal features. According to this study, the greater the power-law index, the more effectively driven and natural mixed convection transport heat. Furthermore, if the Reynolds or Grashof numbers are held constant while changing the Richardson number, the efficiency of heat transmission changes. Pure mixed convection in lid driven enclosure has been simulated by Chowdhury et al.[35]. They considered the power-law model.

Moreover, Ali, I. R.[36] utilized a hybrid nanofluid consisting of $Al2O3 - Cu -$ Water in a double moving wall quadrilateral enclosure to improve the transmission of heat during this investigation he employed Finite Volume Method (FVM) for results. The SIMPLE algorithm is used to address the pressure–velocity coupling. The results show that using hybrid nanofluid in a tall enclosure significantly improves heat transmission. Additionally, it is observed that a larger solid body can further improve heat transfer at higher Reynolds numbers. Thermal transmission is found to increase with increasing Richardson number. In relation to that

Gangawane[37] investigates the impact of the position of a heated triangular obstacle positioned along the vertical centerline of a top wall moving square domain on the properties of mixed convection. The analysis considers a 2D, laminar, time independent flow of a Newtonian and incompressible fluid. The cavity's upper and lower walls are considered adiabatic, whereas the left and right walls have an ambient temperature (Tc). Hossain[38] examines a 2D mixed convection flow of an incompressible and viscous fluid with viscosity depending upon the temperature past an impermeable upright surface. Perturbation techniques are utilized to solve the reduced equations in the forced and free convection regimes. The numerical outcomes are shown in relation to the local edge heat flux and shear stress.

In recent studies, various numerical and computational techniques have been employed to enhance the understanding of fluid dynamics and related fields. For example, Refaie Ali et al.[42] investigated the enhancement of hydrodynamic forces through miniaturized control of square cylinders using the lattice Boltzmann method. Additionally, another study by Refaie Ali et al.[43] presented an AI-based predictive approach using CFD-ANN and Levenberg–Marquardt in the context of a driven-cavity of Ostwald de-Waele fluid. Furthermore, Majeed et al.[44] conducted numerical simulations to evaluate energy storage performance in a close configuration using Galerkin finite element-based computation. Studies like these, along with others focusing on fluid–structure interactions[45], fractional differentiation applications[46], and the properties of new statistical distributions[47], continue to contribute significantly to the field. Research on electrohydrodynamic stability[48], heat and mass transfer in nanofluid flows[49], and the effects of magnetic fields on bio-viscosity flows[50] also provide valuable insights. Recent work has further explored the influence of magnetic fields on mixed convection in fluid systems[52], and symmetry-based analyses of nonlinear mixed convection[51] have advanced the understanding of multi-physical interactions in complex fluid flows. Additionally, research by Al-Showaikh[53] on the effects of non-uniform geometry on peristaltic flow offers new perspectives on fluid dynamics in biomedical applications.

The examination of mixed convection that takes place in a rectangular cavity is the main topic of the current work. The extension from the available studies deals with the presence of three different iso-perimetric shaped heated blocks of circular, square and triangular shape. The objective of the current article is to estimate the effects of different iso-perimetric shapes on heat transfer rates and convection process.

Problem description

A steady, incompressible, and laminar mixed convective flow and thermal transmission in a 2D rectangular domain of length L and height H is considered respectively. A heated block submerged at the geometric center of the domain is maintained at a constant temperature T_H. Figure 1 depicts the physical properties and cartesian coordinate system considered during the inquiry. In Fig. 1, the space coordinates (x, y) and related velocity components (u, v) are also shown. The cavity's top and bottom walls are permitted to move at the same velocity U_{lid} but in opposing directions. The cavity's horizontal walls are thermally insulated. A constant ambient temperature $(T_c < T_H)$ is maintained along the cavity's left and right vertical walls. Calculating the density fluctuation with temperature makes use of the Boussinesq approximation. Radiation and viscous thermal dissipation have been considered to have insignificant effects on heat transmission[39]. Temperature independence is assumed for all the thermophysical characteristics. Consider three shapes Triangle, Circle and Square of same perimeter as heated blocks. As we all know that the perimeter of circle is equal to circumference of the circle which is given as $2\pi r$, where r is the radius of the circle. And the perimeter of Square is acquired as $4x$, where x is the length of each side. Considering the perimeter of triangle fixed, we have computed the values of r and x and obtained two new cases depicted in Fig. 1.

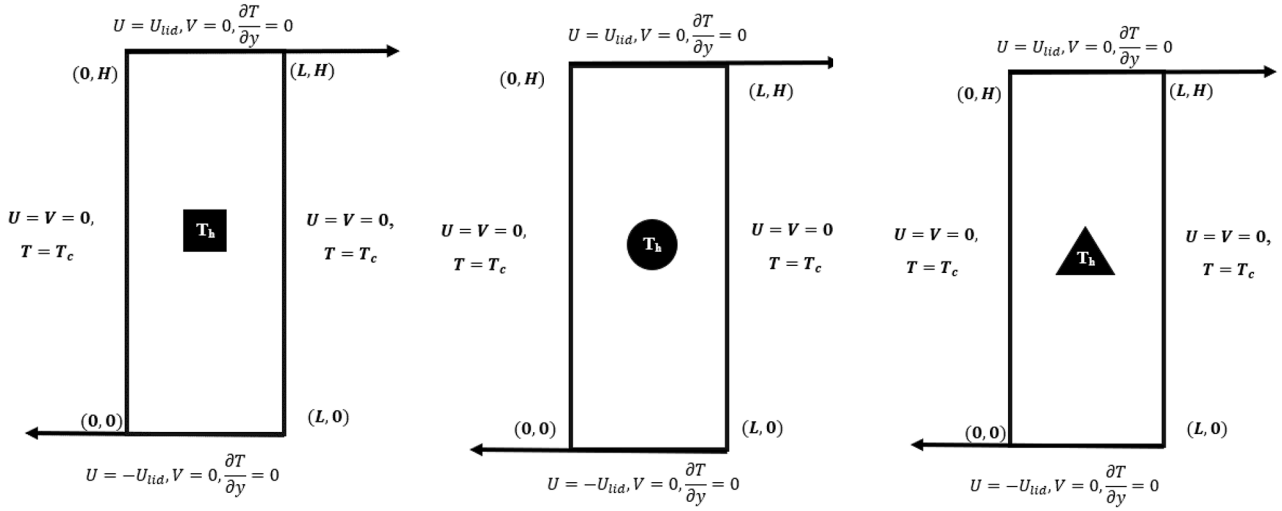

Fig. 1. Schematic diagram of isoperimetric heated blocks.

Mathematical formulation & benchmark quantities

Based on the assumptions stated in previous section, following dimensional governing equations govern the flow dynamics in the cavity:

$$\frac{\partial u}{\partial x}+\frac{\partial v}{\partial y}=0 \tag{1}$$

$$\rho\left[u\frac{\partial u}{\partial x}+v\frac{\partial u}{\partial y}\right]+\frac{\partial p}{\partial x}=\left(\frac{\partial \tau_{xx}}{\partial x}+\frac{\partial \tau_{xy}}{\partial y}\right) \tag{2}$$

$$\rho\left[u\frac{\partial v}{\partial x}+v\frac{\partial v}{\partial y}\right]+\frac{\partial p}{\partial y}=\left(\frac{\partial \tau_{xy}}{\partial x}+\frac{\partial \tau_{yy}}{\partial y}\right)+\rho\beta g(T-T_C) \tag{3}$$

$$\rho c_p\left[u\frac{\partial T}{\partial x}+v\frac{\partial T}{\partial y}\right]=k\left[\frac{\partial^2 T}{\partial x^2}+\frac{\partial^2 T}{\partial y^2}\right] \tag{4}$$

where τ_{ij} is the stress component, $\tau_{ij}=2\mu(\dot{\gamma})\varepsilon_{ij}$

And ε_{ij} is the deformation tensor given as $\varepsilon_{ij}=\frac{1}{2}\left(\frac{\partial u_i}{\partial x_j}+\frac{\partial u_j}{\partial x_i}\right)$, β shows the coefficient of thermal expansion,c_p represents specific heat and k exhibits thermal conductivity, respectively.

Since the model presented in Eqs. (1–4) is non-linear and coupled and each quantity in these equations has its own dimensions. To obtain dimensionless set of equations, we use the following scaling transformations

$$\overline{X}=\frac{x}{H},\overline{Y}=\frac{y}{H},\qquad \overline{U}=\frac{u}{U_{lid}}\ ,\ \overline{V}=\frac{v}{U_{lid}}\ ,\overline{P}=\frac{p}{\rho U_{lid}^2}$$

$$\theta=\frac{T-T_C}{T_H-T_C}$$

The coordinates, components of velocity, pressure, and temperature are all represented in the context by the dimensionless variables $\overline{X},\overline{Y},\overline{U},\overline{V},\overline{P}$ and θ respectively. Putting and arranging the above values in Eqs. (1–4), the following non-dimensional form is obtained:

$$\frac{\partial \overline{U}}{\partial \overline{X}}+\frac{\partial \overline{V}}{\partial \overline{Y}}=0 \tag{5}$$

$$\left[\overline{U}\frac{\partial \overline{U}}{\partial \overline{X}}+V\frac{\partial \overline{U}}{\partial \overline{Y}}\right]+\frac{\partial \overline{P}}{\partial \overline{X}}=\frac{1}{Re}\left(2\frac{\partial}{\partial \overline{X}}\left(\frac{\eta}{m}\frac{\partial \overline{U}}{\partial \overline{X}}\right)+\frac{\partial}{\partial \overline{Y}}\left(\frac{\eta}{m}\left(\frac{\partial \overline{U}}{\partial \overline{Y}}+\frac{\partial \overline{V}}{\partial \overline{X}}\right)\right)\right) \tag{6}$$

$$\left[\overline{U}\frac{\partial \overline{V}}{\partial \overline{X}}+\overline{V}\frac{\partial \overline{V}}{\partial \overline{Y}}\right]+\frac{\partial \overline{P}}{\partial \overline{Y}}=\frac{1}{Re}\left(2\frac{\partial}{\partial \overline{Y}}\left(\frac{\eta}{m}\frac{\partial \overline{V}}{\partial \overline{Y}}\right)+\frac{\partial}{\partial \overline{X}}\left(\frac{\eta}{m}\left(\frac{\partial \overline{U}}{\partial \overline{Y}}+\frac{\partial \overline{V}}{\partial \overline{X}}\right)\right)\right)+Ri\times\theta \tag{7}$$

$$\left[\overline{U}\frac{\partial \theta}{\partial \overline{X}}+\overline{V}\frac{\partial \theta}{\partial \overline{Y}}\right]=\frac{1}{Pr\times Re}\left[\frac{\partial^2\theta}{\partial \overline{X}^2}+\frac{\partial^2\theta}{\partial \overline{Y}^2}\right] \tag{8}$$

where η is the apparent viscosity given as.

$$\eta=m\left\{2\left[\left(\frac{\partial \overline{U}}{\partial \overline{X}}\right)^2+\left(\frac{\partial \overline{V}}{\partial \overline{Y}}\right)^2\right]+\left[\left(\frac{\partial \overline{U}}{\partial \overline{Y}}\right)+\left(\frac{\partial \overline{V}}{\partial \overline{X}}\right)\right]^2\right\}^{\frac{(n-1)}{2}}$$

And the parameters m and n are representing the consistency parameters and power-law indices, respectively. Here $Ri=\frac{Gr}{Re^2}$ is the Richardson number. The generalized expressions for *Pr*, *Re* and *Gr* can be found in[35,36]. These expressions reduce to their classical forms for $n=1$.

Local Nusselt number

The local Nusselt number represents the heat transfer coefficient at a specific point on a surface or within a flow. It is given by the formula:

$$Nu_{Local}=\frac{h\,(x)\,.\mathcal{L}(x)}{\mathcal{K}}$$

where $h\,(x)$ is the local heat transfer coefficient, $\mathcal{L}(x)$ is the characteristic length at the location *x*, and $\mathcal{K}$ is the thermal conductivity of the fluid.

Average Nusselt number

The average Nusselt number is calculated by averaging the local Nusselt numbers over a specified area or length. It provides an overall measure of heat transfer performance for the entire surface or flow. The formula is:

$$Nu_{avg} = \frac{1}{\mathcal{L}} \int_0^{\mathcal{L}} Nu_{Local}\,(x)\,dx$$

where $\mathcal{L}$ is the total length or area over which the average is computed, and $Nu_{Local}(x)$ is the local Nusselt number at position x.

The kinetic energy (KE) is another global secondary quantity that evaluates the scale of momentum for entire flow. The kinetic energy is defined as

$$KE = \frac{1}{2} \int_{\Omega} \langle u.u \rangle\, d\Omega.$$

Solution approach & solvers

For solving the model presented in Eqs. (5)-(8), we have employed Finite Element Method based commercial software COMSOL 5.6 which offer Taylor–Hood family of stable finite elements for the approximation of velocity, temperature and pressure approximations. Moreover, a library offering nonlinear and linear solvers is also available. In the FEM procedure, the physical domain is discretized into a limited number of elements, appropriate element shapes and computation functions are chosen, the elemental equations are put together into an overall set of equations, and these equations are then solved using numerical techniques[40,41]. The fundamental discrete nonlinear system of equations was linearized by using the well-known Newton's technique, and then the resulting linearized inner systems were solved with an exact solver named PARDISO that actually uses the method relies on breaking down matrices into lower and upper triangular matrices commonly known as "LU matrix factorization", which diminishes the number of iterations mandatory to achieve the desired level of accuracy or convergence.

The flow chart representing the finite element method (FEM) is illustrated in Fig.2 .

Figure 3 depicts the coarse computational grid; to show the flow dynamics at the boundaries properly, we have utilized hybrid meshing for better and more accurate results.

A grid independence test was conducted using four grid sizes, as detailed in Table 1. The parameter Nu_{avg} was utilized to quantify the test and the study was performed with $Pr = 10$, and $Ri = 1$ for the circular block case. This configuration ensures that the deviation of selected quantities between grid levels extra fine and extremely fine is negligibly small. Consequently, simulations are executed at extra fine level to optimize computational resources. The table includes the corresponding number of elements (#EL) and total unknowns or degrees of freedom (#DOFs). Table 2 shows the refinement levels, number of elements, and degrees of freedom. The table also shows that for all cases of iso-perimetric blocks namely circle, square, and triangle we have more than 200,000 degrees of freedom (at Extremely fine refinement level). Thus, we can say that they have comparable degrees of freedom for the comparison of results and drawing conclusions regarding the optimal configuration.

Table 3 illustrates the comparison between the current simulation results and those reported by Kumar et al.[39], who studied mixed convection within a lid-driven cavity containing a triangular block. A detailed examination of Table 3, with the same geometric and parametric settings used in this study yields accurate results.

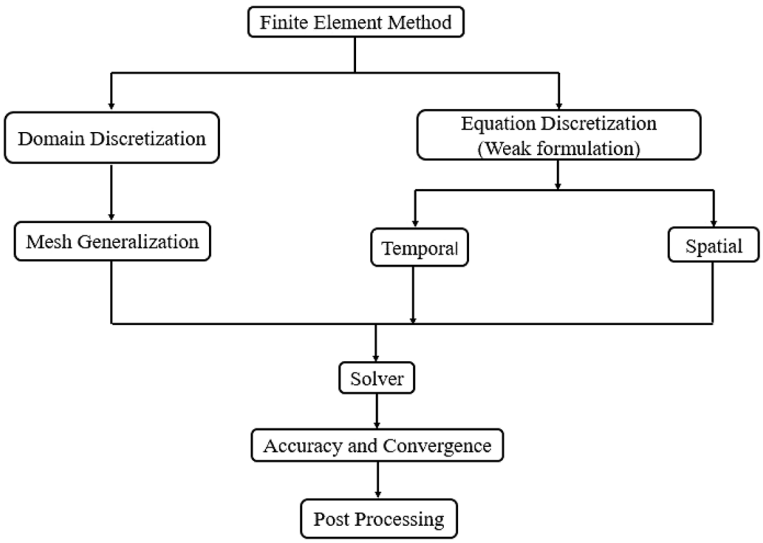

Fig. 2. Flow diagram of finite element method.

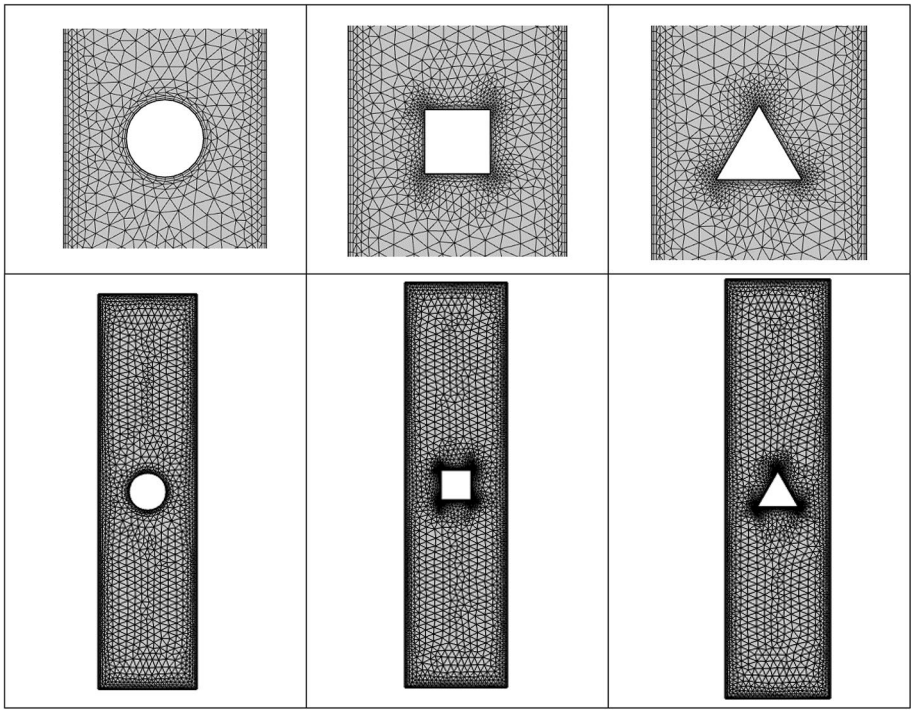

Fig. 3. Coarse refinement level grid.

Levels	#EL	#DOF	Nu_{avg}	% deviation
Normal	5428	12,485	5.137069	–
Fine	9156	20,331	5.152013	0.29
Finer	22,936	50,191	5.191294	0.76
Extra fine	57,026	122,431	5.208933	0.33
Extremely fine	96,252	210,883	5.208293	0.01

Table 1. Grid convergence test for the given problem Pr = 10 and Ri = 1.

	Square block		Circular block		Triangular block	
Refinement level	$\#EL$	$\#DOF$	$\#EL$	$\#DOF$	$\#EL$	$\#DOF$
Extremely Coarse	976	2439	776	2011	930	2339
Extra coarse	1572	3861	1276	3221	1536	3786
Coarser	2476	5899	1946	4751	2432	5793
Coarse	4470	10,337	3548	8365	4340	10,054
Normal	6694	15,165	5428	12,485	6562	14,878
Fine	11,364	24,955	9156	20,331	10,962	24,103
Finer	26,322	57,251	22,936	50,191	26,072	56,683
Extra fine	63,626	136,119	57,026	122,431	62,666	134,066
Extremely fine	104,338	217,543	96,252	210,883	103,214	215,162

Table 2. Refinement levels for different iso-perimetric shapes.

Results and discussions

Through the examination of streamlines and velocity profiles, the convective behavior and properties within the rectangular cavity were investigated, considering the influence of various parameters. These parameters include the Richardson number $(0.1 \leq Ri \leq 10)$, non-Newtonian fluids $(0.6 \leq n \leq 1.4)$, aspect ratio of 0.25 and Prandtl number from $(1, 10)$.

Ri	Current work	Kumar et al.[39]
0.1	4.600314564213044	4.7241
1	4.600316485541422	4.7157
10	4.600316759670698	4.7151

Table 3. Code validation study: comparison of Nu_{avg} with Kumar et al.[39].

The objective of the current numerical simulation was to examine mixed convection in a long, double-wall moving domain that was governed by a lid and comprised three distinct iso-perimetric-shaped blocks that were heated evenly. Numerous parameters, including the coefficient power-law and the Richardson number $(0.1, 1, 10)$, have been seen to have an impact.

The effects of the index $n = (0.6, 1, 1.4)$, Pr $(1, 10)$, and $\text{AR} = 0.25$ on the convective characteristics of the long rectangular cavity have all been investigated. Thermal contours and streamlines are used to examine the convection properties. As viscosity increases and the Prandtl number approaches $Pr = 10$, momentum diffuses more quickly than heat. The isotherm profiles shown in the figure show the combined effects of the moving wall's motion and the convection currents created by buoyancy travelling between the heated blocks and walls. The increase in the power-law index corresponds to an increase in Nu values when $AR = 0.25$ and all other factors are considered.

The two famous dimensionless parameters, Nusselt number (Nu) and Richardson number (Ri), are commonly used in fluid mechanics to describe the characteristics of fluid flow and heat transport. A kind of fluid phenomenon called "mixed convection" mixes free convection with forced convection. The value of the Nusselt number can be influenced by the Richardson number as well as other dimensionless variables like Re and Pr. Specifically, for mixed convection in a rectangular domain, Nu rises as the Ri rises.

Prandtl number also has a highly special relationship with Nu that is crucial in determining the characteristics of heat loss and fluid dynamics. According to their relationship, raising Pr for a given fluid and a certain flow state would result in a rise in the Nusselt number, respectively.

Impact of parameters on velocity profiles:

This section represents the velocity profiles for all three iso-perimetric shaped heated blocks for Aspect Ratio 0.25 and fixed Prandtl number Pr = 1, while other parameters like non-Newtonian fluid index vary from 0.6 to 1.4 and Richardson numbers change from 0.1 to 10.

Figure 4 shows the impact on the velocity of fluid due to the varying values of *n* and *Ri* for different iso-perimetric shaped heated blocks, The velocity is maximum at the lower and upper ends of the cavity due to the no slip boundary condition which is decreases as we move towards the center. Through figure we can also observe that when we increase the indices between 0.6 to 1.4 (from shear thinning to shear thickening) the size and strength of the vortices increases. We do not see any significant change in the velocity profiles by increasing the values of Ri from 0.1 to 10.

Impact of parameters on streamlines

Streamline contours are shown in this section for the three iso-perimetric shaped heated blocks for AR 0.25, with various parameters like power-law index n, *Ri* and *Pr,* respectively.

Streamlines are represented by Fig. 5 for fixed *Pr* = 1 and AR = 0.25 along with different varying parameters (Ri and n). The motion of the lids generates primary vortices at the bottom and top ends of the domain in clockwise and anticlockwise directions, while the obstacle creates secondary vortices. Figure 5 depicts that the strength, size, and quantity of secondary vortices increase along with the values of *Ri* and *n*.

When studying the flow behavior in mixed convection, where both forced and natural forces play a significant role, the Ri is frequently utilized. In mixed convection, buoyancy and shear, both of which are frequently impacted by the kinetic energy of the fluid, drive the fluid motion. *Ri* and kinetic energy have no direct relationship, but the fluid's kinetic energy can influence the fluid's temperature dispersion and the related temperature gradient.

Table 4, 5, 6 represents the values of Nu_{avg} for all three cases of iso-perimetric shaped heated blocks against varying parameters. For circles, Square and Triangles for all these cases Nu_{avg} progressively increases with the enhancement in the values of *Ri* and *n*. And Nu_{avg} also shows an increasing trend with *Pr* from 1 to 10, respectively.

In Table 4, 5, 6, the circular heated block has the greatest influence on Nu_{avg} when compared to the other iso-perimetric shapes.

Table 7, 8, 9 presents the values of KE for a range of parameters. The KE for all three iso-perimetric shaped heated blocks have been represented for different values of *Ri*, *n,* and *Pr* from 1 to 10. The table shows that while keeping other parameters constant, increasing the Pr from 1 to 10 improves the thermal transmission and certainly the Kinetic energy. With the rise in the values of fluid's consistency index from $\text{n} = 0.6$ to 1.4, values of KE significantly increase.

As observed, changing the shape of the heated block affects how rapidly heat is transferred, with circular shape having the most effect. It may be the result of the fluid surrounding a heated circular block becoming buoyant due to the temperature differential. This natural molecular force can cause the fluid to go upward or downward depending on the position, shape and size of the block and the direction of the temperature gradient, which can lead to complex fluid motion around the block.

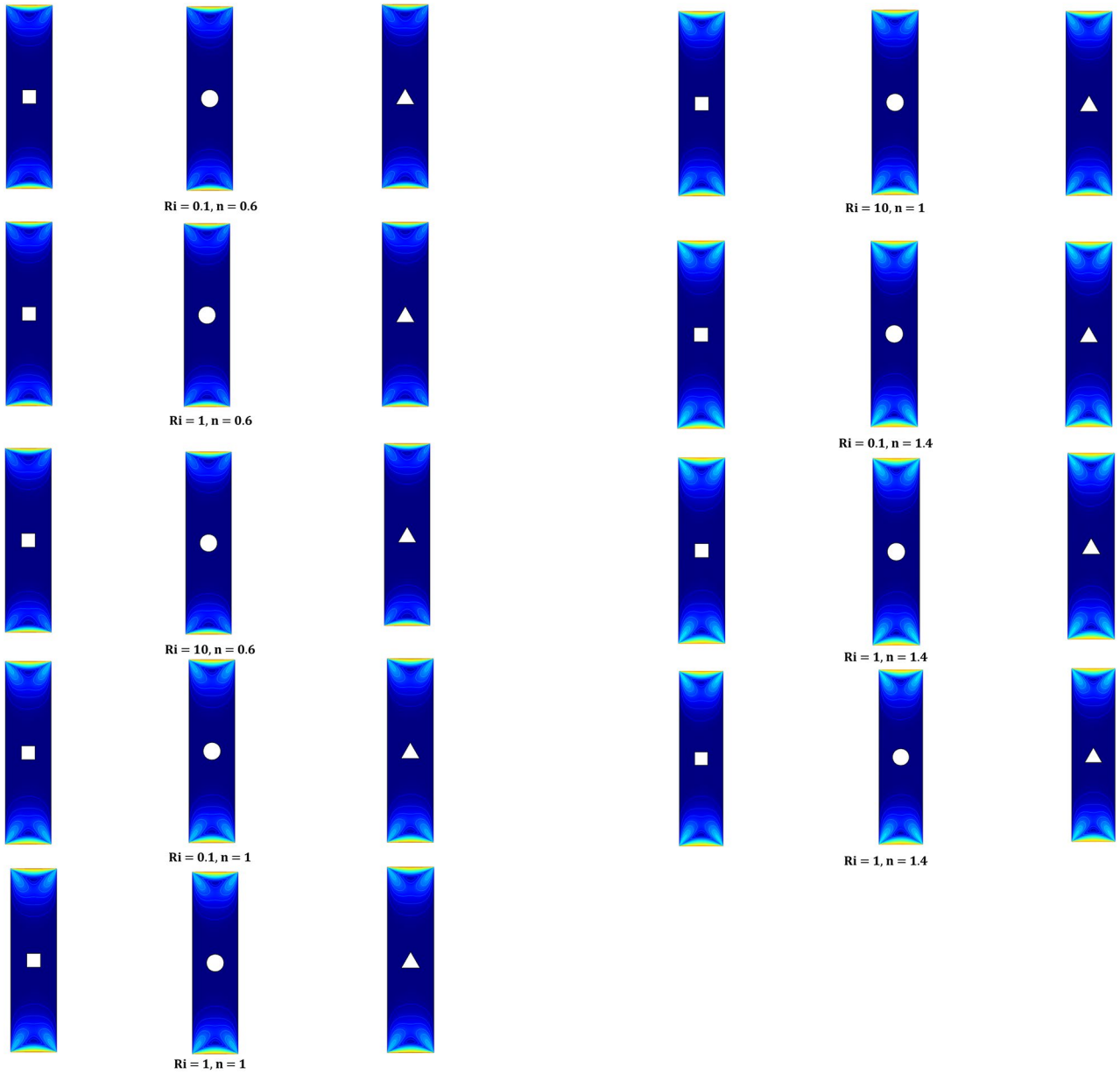

Fig. 4. Variation on velocity profiles for the *Ri* (0.1,1,10), *Pr*=1 and *n* (0.6,1,1.4).

Conclusion

Three iso-perimetric but various-shaped obstacles have been placed in a rectangular enclosure with aspect ratio 1:4 to see the impact of heat transfer and to decide the optimal shape that enhances the heat transfer mechanism. The benchmark quantities of average Nusselt number and kinetic energy values have been computed at various scales of the Prandtl number (*Pr*=1,10), Richardson number ($0.1 \leq Ri \leq 10$), and Power law indices ($0.6 \leq n \leq 1.4$). The findings lead to the following conclusions:

By incrementing in the value of *Pr*, the values of Nu_{avg} increase.
The value of Nu_{avg} increases when the value of *Ri* varies from 0.1 to 10.
Values of Nu_{avg} and KE increases with the increase in the Power law index from 0.6 to 1.4
It has been observed that the Circular heated obstacle had the highest values of Nu_{avg} and KE as compared to the triangular or square heated block. Therefore, we can conclude that the circular shape is the most effective shape for heat transfer in this computational setup.
The effect of *Pr* number is less significant at lower *Ri* values.
The circular shape is superior to the other two in terms of heat transmission efficiency.

In future, this study can be extended to three-dimensional flows involving shape and parametric optimization algorithms for the heated blocks.

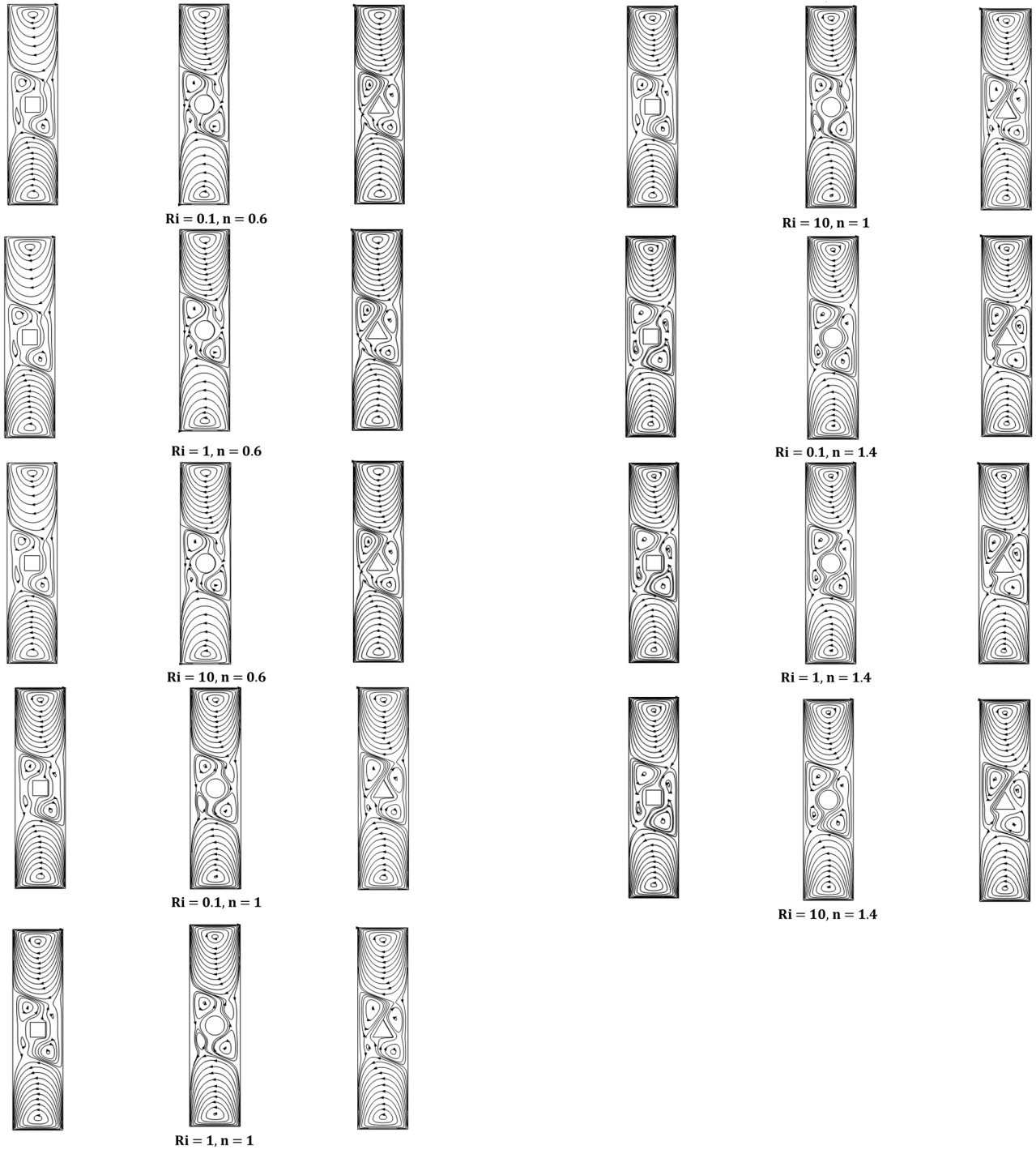

Fig. 5. Variation on streamlines for the *Ri* (0.1,1,10), $Pr = 1$, and *n* (0.6,1,1.4).

Triangular block			
Ri	$n = 0.6$	$n = 1$	$n = 1.4$
$Pr = 1$			
0.1	4.6003126209978245	4.600314564213044	4.60031571068493
1	4.600313717169332	4.600316485541422	4.600323225269491
10	4.600313717610603	4.600316759670698	4.6003232596343775
$Pr = 10$			
0.1	4.600359754877665	4.600388687606466	4.600588461864127
1	4.600360840253299	4.600458619229786	4.600605981426356
10	4.600360840634940	4.600458893474137	4.600606015736777

Table 4. Variation in Nu_{avg} for triangular block.

Circular block			
Ri	$n = 0.6$	$n = 1$	$n = 1.4$
Pr = 1			
0.1	5.2080635250405685	5.207986205207084	5.2080468930227015
1	5.208064765973295	5.208065363577031	5.20806672138569
10	5.208064766563796	5.20806567400318	5.2080667602122
Pr = 10			
0.1	5.208748196021137	5.208758196513681	5.208922582846382
1	5.208749424643913	5.208837373703201	5.2089424174913574
10	5.208749425050214	5.208837684202272	5.208942456322602

Table 5. Variation in Nu_{avg} for circular block.

Square block			
Ri	$n = 0.6$	$n = 1$	$n = 1.4$
Pr = 1			
0.1	4.811289407970605	4.811297930522045	4.811299925365667
1	4.81129055434863	4.811291058268757	4.811302243126531
10	4.811290554958135	4.811291345052082	4.811302278997555
Pr = 10			
0.1	4.812014451849504	4.812019103903576	4.812165304403382
1	4.812015587491476	4.8120922503959225	4.8121836286717805
10	4.812015587901151	4.812092537252813	4.812183664481747

Table 6. Variation in Nu_{avg} for square block.

Triangular block			
Ri	$n = 0.6$	$n = 1$	$n = 1.4$
Pr = 1			
0.1	0.04720643724518969	0.0675661303065068	0.08057750810305506
1	0.047206885310719325	0.0675681842542786	0.08057812227043229
10	0.047206889187151933	0.06756819230903285	0.08057812347193449
Pr = 10			
0.1	0.047206143587818286	0.06756569227419969	0.08057768096276772
1	0.04720889169405125	0.06756774619644185	0.08057869513091456
10	0.04721090303598736	0.06756775425109507	0.08057869633242241

Table 7. Variation in KE for triangular block.

Circular block			
Ri	$n = 0.6$	$n = 1$	$n = 1.4$
Pr = 1			
0.1	0.04725910551169377	0.06757649679653465	0.08058264400484288
1	0.04729984570024966	0.0675785507563644	0.08058525818674172
10	0.04729987440851826	0.06757855881115656	0.08058995938827212
Pr = 10			
0.1	0.0473880652011413	0.067593429633011186	0.08059864810662241
1	0.04738822553449027	0.06759634931649592	0.0805992619679327
10	0.04738872451466285	0.06759935736749064	0.08059996316880193

Table 8. Variation in KE for circular block.

Square block			
Ri	$n = 0.6$	$n = 1$	$n = 1.4$
Pr = 1			
0.1	0.04720736281531378	0.06756753988364314	0.08057892870481691
1	0.04721210599811218	0.06756959387455652	0.08057954289574767
10	0.0472150044599164	0.0675696019294787	0.08057960109731186
Pr = 10			
0.1	0.047280436261529665	0.06757097815576746	0.08058025762622526
1	0.04729519518174297	0.06757303103577754	0.08058087146748723
10	0.047305094120620334	0.06757313908635284	0.08058088266834992

Table 9. Variation in KE for square block.

Data availability

Data will be available on request by contacting the corresponding author, Dr. Ahmed Refaie Ali, via ahmed.refaie@science.menofia.edu.eg , OR via Dr. Afraz Hussain Majeed at afraz@ujs.edu.cn .

Received: 19 May 2024; Accepted: 31 October 2024
Published online: 15 November 2024

References

1. de Vahl Davis, G. Laminar natural convection in an enclosed rectangular cavity. *Int. J. Heat Mass Transf.* **11**(11), 1675–1693 (1968).
2. de Vahl Davis, G. Natural convection of air in a square cavity: a bench mark numerical solution. *Int. J. Numer. Meth. Fluids* **3**(3), 249–264 (1983).
3. Roy, S. & Basak, T. Finite element analysis of natural convection flows in a square cavity with non-uniformly heated wall (s). *Int. J. Eng. Sci.* **43**(8–9), 668–680 (2005).
4. Selimefendigil, F. & Öztop, H. F. MHD mixed convection of nanofluid in a flexible walled inclined lid-driven L-shaped cavity under the effect of internal heat generation. *Physica A* **534**, 122144 (2019).
5. Zhu, Z. J. & Yang, H. X. Numerical investigation of transient laminar natural convection of air in a tall cavity. *Heat Mass Transf.* **39**, 579–587 (2003).
6. Öztop, H. F. & Dagtekin, I. Mixed convection in two-sided lid-driven differentially heated square cavity. *Int. J. Heat Mass Transf.* **47**(8–9), 1761–1769 (2004).
7. Wakitani, S. Flow patterns of natural convection in an air-filled vertical cavity. *Phys. Fluids* **10**(8), 1924–1928 (1998).
8. D'Orazio, M. C., Cianfrini, C. & Corcione, M. Rayleigh-Bénard convection in tall rectangular enclosures. *Int. J. Therm. Sci.* **43**(2), 135–144 (2004).
9. Lartigue, B., Lorente, S. & Bourret, B. Multicellular natural convection in a high aspect ratio cavity: Experimental and numerical results. *Int. J. Heat Mass Transf.* **43**(17), 3157–3170 (2000).
10. Basak, T., Roy, S., Sharma, P. K. & Pop, I. Analysis of mixed convection flows within a square cavity with uniform and non-uniform heating of bottom wall. *Int. J. Therm. Sci.* **48**(5), 891–912 (2009).
11. Javed, T., Mehmood, Z. & Pop, I. MHD-mixed convection flow in a lid-driven trapezoidal cavity under uniformly/non-uniformly heated bottom wall. *Int. J. Numer. Meth. Heat Fluid Flow* **27**(6), 1231–1248 (2017).
12. Lamsaadi, M., Naimi, M., Hasnaoui, M. & Mamou, M. Natural convection in a vertical rectangular cavity filled with a non-Newtonian power law fluid and subjected to a horizontal temperature gradient. *Numer. Heat Transf. Part A Appl.* **49**(10), 969–990 (2006).
13. Mendu, S. S. & Das, P. K. Flow of power-law fluids in a cavity driven by the motion of two facing lids–A simulation by lattice Boltzmann method. *J. Nonnewton. Fluid Mech.* **175**, 10–24 (2012).
14. Raizah, Z. A. S., Aly, A. M. & Ahmed, S. E. Natural convection flow of a power-law non-Newtonian nanofluid in inclined open shallow cavities filled with porous media. *Int. J. Mech. Sci.* **140**, 376–393 (2018).
15. Souayeh, B., Ben-Cheikh, N. & Ben-Beya, B. Effect of thermal conductivity ratio on flow features and convective heat transfer. *Part. Sci. Technol.* **35**(5), 565–574 (2017).
16. Souayeh, B., Ben-Cheikh, N. & Ben-Beya, B. Periodic behavior flow of three-dimensional natural convection in a titled obstructed cubical enclosure. *Int. J. Numer. Meth. Heat Fluid Flow* **27**(9), 2030–2052 (2017).

17. Souayeh, B., Hammami, F., Hdhiri, N. & Alfannakh, H. Unsteady state fluid structure of two-sided nonfacing lid-driven cavity induced by a semicircle at different radii sizes and velocity ratios. *Int. J. Mod. Phys. C* **30**(08), 1950060 (2019).
18. Hammami, F., Souayeh, B., Ben-Cheikh, N. & Ben-Beya, B. Computational analysis of fluid flow due to a two-sided lid driven cavity with a circular cylinder. *Comput. Fluids* **156**, 317–328 (2017).
19. Souayeh, B., Alam, M. W., Hammami, F., Hdhiri, N. & Yasin, E. Predicting the unsteady states of 2D and 3D lid-driven cavities induced by a centrally located circle and sphere. *Fluid Dyn. Res.* **52**(2), 025507 (2020).
20. Gangawane, K. M. & Gupta, S. Mixed convection characteristics in rectangular enclosure containing heated elliptical block: Effect of direction of moving wall. *Int. J. Therm. Sci.* **130**, 100–115 (2018).
21. Elboughdiri, N., Sohail, M., Nazir, U., Elmasry, Y. & Hassan, A. M. Significance of heat passage in four-phase Oldroyd-B nanofluid with solar thermal radiations through a cone: A study of entropy analysis. *Case Stud. Therm. Eng.* **53**, 103849 (2024).
22. Sohail, M., Nazir, U., Singh, A., Tulu, A. & Khan, M. J. Finite element analysis of cross fluid model over a vertical disk suspended to a tetra hybrid nanoparticles mixture. *Sci. Rep.* **14**(1), 1520 (2024).
23. Elboughdiri, N., Nazir, U., Saleem, S. & Ali, M. R. Impact of thermal energy efficiency based on kerosene oil movement through hybrid nano-particles across contracting/stretching needle. *Case Studies in Thermal Engineering* **60**, 104775 (2024).
24. Sohail, M. et al. Utilization of Galerkin finite element strategy to investigate comparison performance among two hybrid nanofluid models. *Sci. Rep.* **12**(1), 18970 (2002).
25. Billah, M. M. et al. Numerical analysis of fluid flow due to mixed convection in a lid-driven cavity having a heated circular hollow cylinder. *Int. Commun. Heat Mass Transfer* **38**(8), 1093–1103 (2011).
26. Islam, A. W., Sharif, M. A. & Carlson, E. S. Mixed convection in a lid driven square cavity with an isothermally heated square blockage inside. *Int. J. Heat Mass Transf.* **55**(19–20), 5244–5255 (2012).
27. Manchanda, M. & Gangawane, K. M. Mixed convection in a two-sided lid-driven cavity containing heated triangular block for non-Newtonian power-law fluids. *Int. J. Mech. Sci.* **144**, 235–248 (2018).
28. Vijayan, A. & Gangawane, K. M. Mixed convection in a tall lid-driven cavity with a triangular heat source for non-Newtonian power-law fluids. *J. Therm. Anal. Calorim.* **146**, 937–954 (2021).
29. Cheng, T. S. Characteristics of mixed convection heat transfer in a lid-driven square cavity with various Richardson and Prandtl numbers. *Int. J. Therm. Sci.* **50**(2), 197–205 (2011).
30. Laidoudi, H. & Ameur, H. Investigation of the mixed convection of power-law fluids between two horizontal concentric cylinders: Effect of various operating conditions. *Therm. Sci. Eng. Prog.* **20**, 100731 (2020).
31. Thohura, S., Molla, M. M., Sarker, M. A. & Paul, M. C. Study of mixed convection flow of power-law fluids in a skewed lid-driven cavity. *Heat Transf.* **50**(6), 6328–6357 (2021).
32. Rehman, N., Mahmood, R., Majeed, A. H., Rehman, K. U. & Shatanawi, W. Finite element analysis on entropy generation in MHD iron (III) oxide-water nanofluid equipped in partially heated fillet cavity. *J. Magnet. Magnet. Mater.* **565**, 170269 (2023).
33. Safaei, M. R., Rahmanian, B. & Goodarzi, M. Numerical study of laminar mixed convection heat transfer of power-law non-Newtonian fluids in square enclosures by finite volume method. *Int. J. Phys. Sci.* **6**(33), 7456–7470 (2011).
34. Roy, P. P., Chowdhury, S., Raj, M. H., Islam, M. Q. & Saha, S. Forced, natural and mixed convection of non-Newtonian fluid flows in a square chamber with moving lid and discrete bottom heating. *Results Eng.* **17**, 100939 (2023).
35. Chowdhury, S., Roy, P. P., Raj, M. H. & Saha, S. Pure mixed convection in a Non-Newtonian fluid filled lid-driven chamber with discrete bottom heating. *Case Stud. Therm. Eng.* **49**, 103183 (2023).
36. Ali, I. R., Alsabery, A. I., Bakar, N. A. & Roslan, R. Mixed convection in a double lid-driven cavity filled with hybrid nanofluid by using finite volume method. *Symmetry* **12**(12), 1977 (2020).
37. Gangawane, K. M., Öztop, H. F. & Abu-Hamdeh, N. Mixed convection characteristic in a lid-driven cavity containing heated triangular block: Effect of location and size of block. *Int. J. Heat Mass Transf.* **124**, 860–875 (2018).
38. Hossain, M. A. & Munir, M. S. Mixed convection flow from a vertical flat plate with temperature dependent viscosity. *International Journal of Thermal Sciences* **39**(2), 173–183 (2000).
39. Kumar, S., Gangawane, K. M. & Öztop, H. F. A numerical study of mixed convection in a two-sided lid-driven tall cavity containing a heated triangular block for non-Newtonian power-law fluids. *Heat Transf.* **50**(5), 4806–4829 (2021).
40. Rehman, N., Mahmood, R., Majeed, A. H., Ali, M. R. & Hendy, A. S. Enhanced heat transfer in vented square enclosures with block structures: Exploring iso-perimetric shapes and multigrid approach for mixed convection of nano-fluids. *Case Stud. Therm. Eng.* **58**, 104391 (2024).
41. Mahmood, R. et al. Numerical computations of entropy generation and MHD ferrofluid filled in a closed wavy configuration: finite element based study. *Front. Phys.* **10**, 916394 (2022).
42. Refaie Ali, A. et al. Enhancing hydrodynamic forces through miniaturized control of square cylinders using the lattice Boltzmann method. *Sci. Rep.* **14**, 15524. https://doi.org/10.1038/s41598-024-65423-4 (2024).
43. Refaie Ali, A. et al. AI-based predictive approach via FFB propagation in a driven-cavity of Ostwald de-Waele fluid using CFD-ANN and Levenberg–Marquardt. *Sci. Rep.* **14**, 11024. https://doi.org/10.1038/s41598-024-60401-2 (2024).
44. Majeed, A. H. et al. Numerical simulations of energy storage performance in a close configuration: A Galerkin finite element-based computation. *Alex. Eng. J.* **104**, 56–65. https://doi.org/10.1016/j.aej.2024.06.037 (2024).
45. Hussin, A. M. Numerical simulation of fluid-structure interactions on super-tall slender structures using two-way coupling techniques. *Appl. Math. Inf. Sci.* **18**(5), 1125–1140. https://doi.org/10.18576/amis/180518 (2024).
46. Irgashev, B. Solution of an initial value problem of Cauchy type for one equation. *Prog. Fract. Differ. Appl.* **10**(1), 113–118. https://doi.org/10.18576/pfda/100111 (2024).
47. Sayibu, S., Luguterah, A., & Nasiru, S. McDonald generalized power WeiBull distribution: Properties, and applications. *J. Stat. Appl. Prob.* **13**(1), 297–322. https://doi.org/10.18576/jsap/130121 (2024).
48. Elazab, S. S. & Hasan, A. A. Electrohydrodynamic stability of self-gravitating fluid cylinder. *Inf. Sci. Lett.* **13**(1), 1–10. https://doi.org/10.18576/isl/130101 (2024).
49. Kumar, K., Singh, B., Kumar, P., Nisar, K.S., Abdel-Aty, A.H., Alkhazaleh, S. & Abdel-Aty, M. Heat and mass transfer effect in stagnation point flow of MHD Jeffery nanofluid flow over porous stretching sheet with thermal radiation. *Int. J. Thin Films Sci. Technol.* **13**(1), 47–58. https://doi.org/10.18576/ijtfst/130106 (2024).
50. Ali, A. R. et al. Exploring magnetic and thermal effects on MHD bio-viscosity flow at the lower stagnation point of a solid sphere using Keller box technique. *Partial Differ. Equ. Appl. Math.* **9**, 100601. https://doi.org/10.1016/j.padiff.2023.100601 (2024).
51. Saleem, M., Majeed, A. H., Ahmad, I. & Ali, A. R. Symmetry-based analysis of nonlinear mixed convection in 3D EMHD nano-Carreau fluid flow with Riga stretched surface effects and multi-physical interactions. *ZAMM-J. Appl. Math. Mech./Z. Angew. Math. Mech.* https://doi.org/10.1002/zamm.202400072 (2024).
52. Mahmuda Maya, M. U., Alam, M. N. & Refaie Ali, A. Influence of magnetic field on MHD mixed convection in lid-driven cavity with heated wavy bottom surface. *Sci. Rep.* **13**, 18959. https://doi.org/10.1038/s41598-023-45707-x (2023).
53. Al-Showaikh, F. N. M. The exact endoscopic effect and non-uniform geometry on the peristaltic flow. *Appl. Math. Inf. Sci.* **18**(5), 1029–1035. https://doi.org/10.18576/amis/180510 (2024).

Acknowledgements
We are grateful for the open access funding provided by The Science, Technology & Innovation Funding Authority (STDF) in partnership with The Egyptian Knowledge Bank (EKB). STDF's support allows us to share our research with a global audience, promoting collaboration and advancing scientific knowledge.

Author contributions
All authors listed have significantly contributed to the development and the writing of this article and all authors are participated equally in this research paper.

Funding
Open access funding is provided by The Science, Technology & Innovation Funding Authority (STDF) in collaboration with The Egyptian Knowledge Bank (EKB).

Additional information
Correspondence and requests for materials should be addressed to A.R.A.